

# Photohadronic scenario in interpreting the February–March 2014 flare of 1ES 1011+496

Sarira Sahu<sup>1,2,a</sup>, Alberto Rosales de León<sup>1,b</sup>, Luis Salvador Miranda<sup>3,c</sup>

<sup>1</sup> Instituto de Ciencias Nucleares, Universidad Nacional Autónoma de México, Circuito Exterior, C.U., A. Postal 70-543, 04510 Mexico, DF, Mexico

<sup>2</sup> Astrophysical Big Bang Laboratory, RIKEN, Hirosawa, Wako, Saitama 351-0198, Japan

<sup>3</sup> Department of Physics, University of Johannesburg, P.O. Box 524, Auckland Park 2006, South Africa

Received: 19 September 2017 / Accepted: 26 October 2017 / Published online: 6 November 2017  
© The Author(s) 2017. This article is an open access publication

**Abstract** The extraordinary multi-TeV flare from 1ES 1011+496 during February–March 2014 was observed by the MAGIC telescopes for 17 nights and the average spectrum of the whole period has a non-trivial shape. We have used the photohadronic model and a template extragalactic background light model to explain the average spectrum which fits the flare data well. The spectral index  $\alpha$  is the only free parameter in our model. We have also shown that the non-trivial nature of the spectrum is due to the change in the behavior of the optical depth above  $\sim 600$  GeV  $\gamma$ -ray energy accompanied with the high SSC flux. This corresponds to an almost flat intrinsic flux for the multi-TeV  $\gamma$ -rays. Our model prediction can constrain the SSC flux of the leptonic models in the quiescent state.

## 1 Introduction

The 1ES 1011+496 (RA: 153.767°, DEC: 49.434°) is a high frequency peaked BL Lac (HBL) object at a redshift of  $z = 0.212$ . This HBL was discovered at very high energy (VHE)  $> 100$  GeV by the MAGIC telescopes in 2007 following an optical high state reported by the Tuorla Blazar Monitoring Program [1]. Two more multi-wavelength observations of the HBL were carried out by the MAGIC telescopes in 2008 [2] and in 2011–2012 [3]. During these two observation periods the source did not show any flux variability. On 5th February 2014, the VERITAS collaboration [4] issued an alert about the flaring of 1ES 1011+496, which was immediately followed by the MAGIC telescopes from February 6th to March 7th, a total of 17 nights [5]. The flare

was observed in the energy range  $\sim 75$ –3100 GeV and the flux could reach values more than 10 times higher than any previously recorded flaring state of the source [1,6]. Despite this large variation, no significant intra-night variability was observed in the flux. This allowed the collaboration to use the average of the 17 nights observed spectral energy distribution (SED) to look for the imprint of the extragalactic background light (EBL) induced  $\gamma$ -rays absorption on it [5].

The SEDs of the HBLs have a double peak structure in the  $\nu$ – $\nu F_\nu$  plane. While the low energy peak corresponds to the synchrotron radiation from a population of relativistic electrons in the jet, the high energy peak is believed to be due to the synchrotron self Compton (SSC) scattering of the high energy electrons with their self-produced synchrotron photons. The so-called leptonic model, which incorporates both the synchrotron and the SSC processes in it, is very successful in explaining the multi-wavelength emission from blazars and FR I galaxies [7–12]. However, difficulties arise in explaining the multi-TeV (very hard  $\gamma$ -rays) emission from Cen A [13], flares from the radio galaxy M87 [14], the flares from 1ES 1959+650 [15,16] and Markarian 421 (Mrk 421) [17]. Also a direct consequence of the leptonic scenario is that emission in the multi-TeV energy range has to be accompanied by a simultaneously enhanced emission in the synchrotron peak. Unfortunately this enhanced synchrotron emission was not observed in the flaring of 1ES 1959+650 in June 2002 [15] and also in the flaring of Mrk 421 in April 2004 [17], which implies that the SSC model may not be efficient enough to contribute in the multi-TeV regime.

The observation of very hard  $\gamma$ -rays from distant blazars also poses a challenge to the traditional SSC model, a hint for alternative scenarios. In this context different hadronic models are developed to explain the VHE emission from these objects. Cao et al. [18] have shown that the interaction

<sup>a</sup> e-mail: sarira@nucleares.unam.mx

<sup>b</sup> e-mail: albertoros4@ciencias.unam.mx

<sup>c</sup> e-mail: smiranda-palacios@uj.ac.za

of high energy protons with the synchrotron photons in the jet can produce  $\gamma$ -rays from  $\pi^0$  decay and can explain the multi-TeV emission from 1ES 1011-232. Also Zdziarski et al. [19,20] have used the hadronic model to explain the broad band spectra of radio-loud AGN. However, both the above scenarios require super Eddington luminosity in protons to explain the multi-TeV emission. Again, synchrotron emission from the ultra high energy protons in the jet magnetic field can explain the VHE  $\gamma$ -ray SED [21] which needs a stronger magnetic field at the emission site. In an alternative scenario, ultra high energy protons escaping from the jet region produce VHE photons by interacting with the cosmic microwave background (CMB) photons and/or EBL, which avoids the absorption in the inner jet region [22]. This explains the transparency of the universe to VHE  $\gamma$ -rays due to their proximity to the Earth compared to the one produced in the source which travels a longer distance. Also the TeV spectrum is independent of the intrinsic spectrum but depends on the output of the high energy cosmic rays in the source. This model fits very well the multi-TeV spectra from many sources [23–28]. However, in this scenario, it is assumed that the source produces VHE protons with energies  $10^{17}$ – $10^{19}$  eV, and a weak extragalactic magnetic field in the range  $10^{-17} G < B < 10^{-14} G$  is needed. The photohadronic model is also proposed to explain the multi-TeV emission from HBLs [29–31].

## 2 EBL models

The light produced from all the sources in the universe throughout the cosmic history pervades the intergalactic space which is now at longer wavelengths due to the expansion of the universe and absorption/re-emission by dust and the light in the band 0.1–100  $\mu\text{m}$  is called diffuse EBL [32]. The observed VHE spectrum of the distant sources is attenuated by EBL producing  $e^+e^-$  pairs. While the EBL is problematic for the study of high redshift VHE  $\gamma$ -ray sources, at the same time the observed VHE  $\gamma$ -ray SED provides an indirect method to probe the EBL. The relation between the intrinsic VHE flux  $F_{\gamma,\text{int}}$  and the observed one  $F_{\gamma,\text{obs}}$  are related through [32,33]

$$F_{\gamma,\text{obs}}(E_\gamma) = F_{\gamma,\text{int}}(E_\gamma) e^{-\tau_{\gamma\gamma}(E_\gamma,z)}, \quad (1)$$

where  $\tau_{\gamma\gamma}$  is the optical depth. As the HBL 1ES 1011+496 is at an intermediate redshift, the observation of the VHE flare from it will provide a good opportunity to study the EBL effect.

A major challenge to extract EBL information from the observed multi-TeV spectrum is our lack of proper understanding of the intrinsic spectrum. Also the gamma-rays produced in the jet region can be absorbed due to pair production

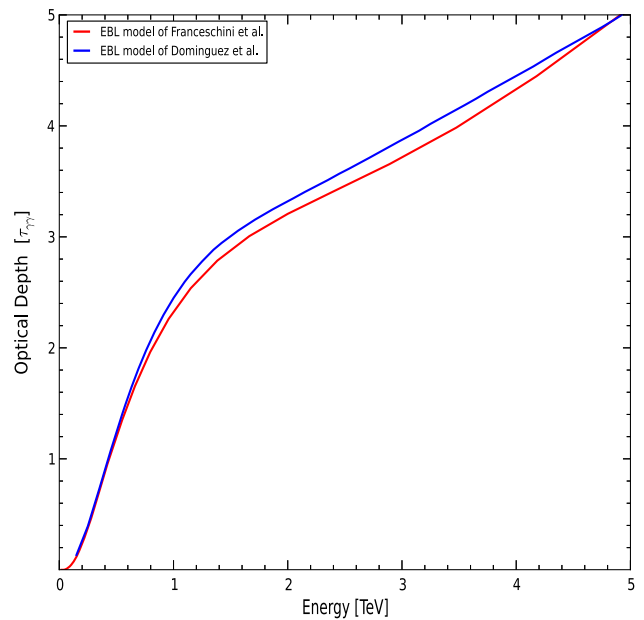


**Fig. 1** At a redshift of  $z = 0.212$ , the optical depths  $\tau_{\gamma\gamma}$  in the EBL models of Domínguez et al. and Franceschini et al. are shown for comparison

with the background photons in the jet. So a better understanding of the emission mechanisms in the jet is desirable. It is hoped that the modeling of the blazar SED by taking into account the emission mechanisms can overcome this intrinsic extraneous effect.

Although a large number of different EBL models exist [33–37], here we shall discuss the two important models by Franceschini et al. [36] and Domínguez et al. [33,37], which are widely used by Imaging Atmospheric Cherenkov Telescopes (IACTs) to constrain the imprint of the EBL on the propagation of the VHE  $\gamma$ -rays by IACTs. We compared  $\tau_{\gamma\gamma}$  of both these models (the central value of the former model is used) for  $E_\gamma < 5$  TeV and found a very small difference as shown in Fig. 1. So for our analysis here we only consider the model due to Domínguez et al. However, the results will be similar for the other one. There are three distinct regions of  $E_\gamma$  in Fig. 1, where the behavior of  $\tau_{\gamma\gamma}$  is different. Below  $E_\gamma \sim 600$  GeV it has a rapid growth. In the energy range  $\sim 600$  GeV to  $\sim 1.2$  TeV the growth is slow and above  $\sim 1.2$  TeV the growth is almost linear. This growth pattern of  $\tau_{\gamma\gamma}$  in different energy domains influences the  $F_{\gamma,\text{obs}}$ , which again depends on the SSC flux of the leptonic models. In the next section we discuss two different leptonic models which are used here to fit the low energy SED of the HBL we study.

## 3 Leptonic models

Different leptonic models are used to fit the low energy SED (synchrotron and SSC) of the HBL 1ES 1011+496. We deal

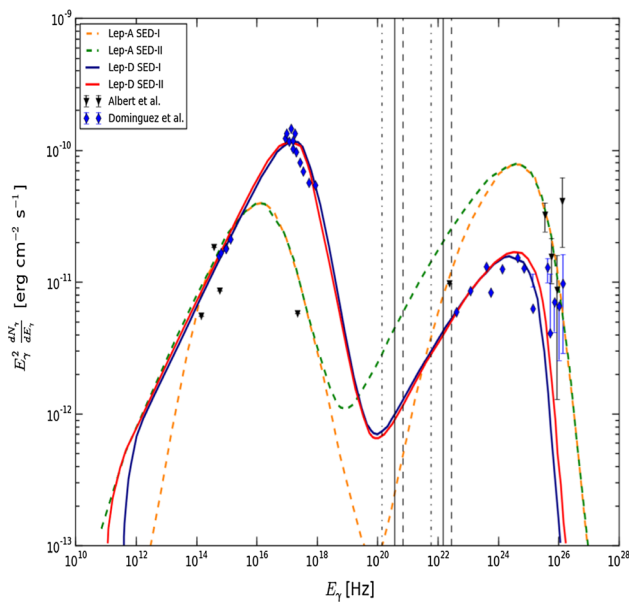


**Fig. 2** The leptonic SED of the HBL 1ES 1011+496 is shown by using the two different models due to Albert et al. [1] and Domínguez et al. [37]. Each of these models has two different parametrizations, which we call SED-I and SED-II. Also the regions in the SED where the VHE protons interact with the SSC photons to produce the multi-TeV flare are shown: the region between the two dashed dotted vertical lines corresponds to SED-II of Domínguez et al., with  $\mathcal{D} = 9.1$ , the region between the two continuous vertical lines corresponds to SED-I of Domínguez et al. with  $\mathcal{D} = 14.6$  and the region between the two vertical dashed lines corresponds to SED-I, II of Albert et al. with  $\mathcal{D} = 20$

with two different leptonic models, by Albert et al. [1] and by Domínguez et al. [37] (hereafter Lep-A and Lep-D, respectively) which explain the low energy SED of the HBL 1ES 1011+496. Below, we briefly discuss these models.

### 3.1 Leptonic model of Albert et al. (Lep-A) [1]

Here the SED is obtained by using the single zone synchrotron-SSC model where the emission region is a spherical blob of radius  $R'_b \sim 10^{16}$  cm and a Doppler factor  $\mathcal{D} = 20$  is taken. The emission region has a magnetic field  $B' \sim 0.15$  G and the relativistic electrons emit synchrotron radiation, which explains the low energy peak of the SED. The high energy emissions from X-rays to few GeV  $\gamma$ -rays are from the Compton scattering of the seed synchrotron photons by the same population of high energy electrons. Here two different parameterizations are used to fit the low energy data and are shown in Fig. 2 as SED-I and SED-II.

### 3.2 Leptonic model of Domínguez et al. (Lep-D) [37]

This leptonic model also uses two different parameterizations to fit the leptonic SED which we call SED-I and SED-II as shown in Fig. 2. The SED-I and SED-II are almost the same

in the SSC energy range. So here we only consider SED-II. However, for SED-I the results will be very similar. The SED-II is fitted by considering the spherical blob of size  $R'_b = 2.2 \times 10^{16}$  cm moving with a bulk Lorentz factor  $\Gamma = 9.1$ . A constant magnetic field  $B' \sim 0.23$  G is present in the blob region where the charged particles undergo synchrotron emission.

## 4 Photohadronic model

We employ the photohadronic model to explain the multi-TeV flaring from many HBLs [21, 29–31, 38]. Here the standard interpretation of the leptonic model is used to explain the low energy peaks. Thereafter, it is proposed that the low energy tail of the SSC photons in the blazar jet serves as the target for the Fermi-accelerated high energy protons, within the jet to produce TeV photons through the decay of  $\pi^0$ s from the  $\Delta$ -resonance [29]. But the efficiency of the photohadronic process depends on the photon density in the blazar jet. In a normal jet, the photon density is low, which makes the process inefficient [20]. However, it is assumed that during the flaring the photon density in the inner jet region can go up so that the  $\Delta$ -resonance production is moderately efficient. Here, the flaring occurs within a compact and confined volume of radius  $R'_f$  (a quantity with ' implies that we describe it in the jet comoving frame) inside the blob of radius  $R'_b$  ( $R'_f < R'_b$ ). The bulk Lorentz factor in the inner jet should be larger than the outer jet. But for simplicity we assume  $\Gamma_{out} \simeq \Gamma_{in} \simeq \Gamma$ . We cannot estimate the photon density in the inner jet region directly as it is hidden. For simplicity, we assume the scaling behavior of the photon densities in different background energies as follows [29–31]:

$$n'_{\gamma,f}(\epsilon'_{\gamma_1})n'^{-1}_{\gamma,f}(\epsilon'_{\gamma_2}) \simeq n'_{\gamma}(\epsilon'_{\gamma_1})n'^{-1}_{\gamma}(\epsilon'_{\gamma_2}). \tag{2}$$

The above equation implies that the ratio of photon densities at two different background energies  $\epsilon'_{\gamma_1}$  and  $\epsilon'_{\gamma_2}$  in the flaring state ( $n'_{\gamma,f}$ ) and in the non-flaring state ( $n'_{\gamma}$ ) remains almost the same. The photon density in the outer region is calculated from the observed flux in the usual way. So the unknown internal photon density is expressed in terms of the known photon density calculated from the observed/fitted SED in the SSC region, which is again related to the observed flux in the same region. This model explains very nicely the observed TeV flux from the orphan flares of 1ES 1959+650, Mrk 421 as well as the multi-TeV flaring from M87 and Mrk 501 [29–31, 39].

In the observer frame, the  $\pi^0$ -decay photon energy  $E_{\gamma}$  and the background SSC photon energy  $\epsilon_{\gamma}$  are related through

$$E_{\gamma}\epsilon_{\gamma} \simeq 0.032 \mathcal{D}^2 (1+z)^{-2} \text{ GeV}^2, \tag{3}$$

where  $E_\gamma$  satisfies the relation  $E_p = 10\Gamma\mathcal{D}^{-1}E_\gamma$ .  $\mathcal{D} \simeq \Gamma$  is the Doppler factor of the relativistic jet and  $E_p$  is the observed proton energy. The intrinsic flux  $F_{\gamma,\text{int}}$  of the flaring blazar is proportional to a power law with an exponential cut-off given as  $E_\gamma^{-\alpha} e^{-E_\gamma/E_{\gamma,c}}$ , with the spectral index  $\alpha \geq 2$ ; the cut-off energy is  $E_{\gamma,c}$  [40]. The effects of both the exponential cut-off and the EBL contribution are to reduce the VHE flux. For far-off sources the EBL plays the dominant role, which shows that  $E_{\gamma,c}$  is much higher than the highest energy  $\gamma$ -ray observed during the VHE flaring event. Recently we have shown [39] that for nearby objects the EBL effect is also important and there is no need of an exponential cut-off. Including the EBL effect in the photohadronic scenario [30] the observed multi-TeV flux is expressed as

$$F_{\gamma,\text{obs}}(E_\gamma) = A_\gamma \Phi_{\text{SSC}}(\epsilon_\gamma) E_{\gamma,\text{GeV}}^{-\alpha+3} e^{-\tau_{\gamma\gamma}(E_\gamma, z)}. \quad (4)$$

The SSC energy  $\epsilon_\gamma$  and the observed energy  $E_\gamma$  satisfy the condition given in Eq. (3),  $\Phi_{\text{SSC}}(\epsilon_\gamma)$  is the SSC flux corresponding to the energy  $\epsilon_\gamma$ ,  $E_{\gamma,\text{GeV}}$  implies  $E_\gamma$  expressed in units of GeV, and  $A_\gamma$  is the dimensionless normalization constant calculated from the observed flare data [30]. The spectral index  $\alpha$  is the only free parameter here. By comparing Eqs. (1) and (4),  $F_{\gamma,\text{int}}$  can be obtained.

## 5 Results

The MAGIC collaboration fitted the average of the 17 nights observed SEDs of HBL 1ES 1011+496 with several functions, however, none of these fit well, due to the non-trivial nature in the VHE limit. Also the intrinsic SED is calculated by subtracting the EBL contribution from the observed flux and is fitted with a simple power law. We use the photohadronic scenario to interpret this flaring. The input for the photohadronic process comes from the leptonic model, i.e.  $\Gamma$ ,  $\Phi_{\text{SSC}}$ , and magnetic field etc. The results of the above two leptonic models, Lep-A and Lep-D, are discussed separately below.

In the hadronic model alluded to previously and using the parameters of the Lep-A, the observed multi-TeV  $\gamma$ -rays in the energy range  $75.6\text{ GeV} \leq E_\gamma \leq 3.1\text{ TeV}$  corresponds to the Fermi-accelerated proton energy in the range  $0.76\text{ TeV} \leq E_p \leq 31\text{ TeV}$  which collides with the SSC photons in the inner jet region in the energy range  $115\text{ MeV} (2.8 \times 10^{22}\text{ Hz}) \geq \epsilon_\gamma \geq 2.8\text{ MeV} (6.8 \times 10^{20}\text{ Hz})$  to produce the  $\Delta$ -resonance and its decay to  $\pi^0$ s produces observed multi-TeV  $\gamma$ -rays. Using the scaling behavior of Eq. (2), the photon densities in the inner and the outer regions of the jet can be related. In the outer region, the above range of  $\epsilon_\gamma$  corresponds to the low energy tail of the SSC photons (energy range between two dashed vertical lines in Fig. 2). We observe that  $\Phi_{\text{SSC}}$  for SED-II is always larger than the cor-

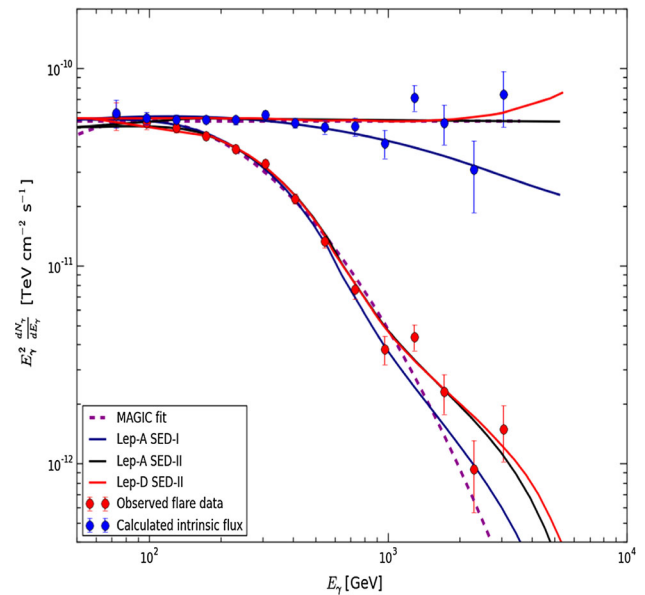


**Fig. 3** Using the leptonic models of Albert et al. (Lep-A) and Domínguez et al. (Lep-D) with the EBL correction, the multi-TeV flare data are fitted in the photohadronic model (lower curves) and the corresponding intrinsic fluxes are also shown (upper curves). The lower and the upper curves of the same color belong to a single model. For comparison the MAGIC fit to the observed flux (lower magenta dashed curve) and the intrinsic flux (upper magenta dashed curve) are shown

responding flux of SED-I. As we know from Eq. (4),  $F_{\gamma,\text{obs}}$  is proportional to  $\Phi_{\text{SSC}}$ , so with the inclusion of the EBL contribution the calculated  $F_{\gamma,\text{obs}}$  with SED-II is always  $\geq$  the flux with SED-I in the above range of  $\epsilon_\gamma$ .

The  $F_{\gamma,\text{obs}}$  and the  $F_{\gamma,\text{int}}$  for SED-I in Lep-A are plotted as functions of  $E_\gamma$  in Fig. 3. A good fit to the flare data is obtained for the normalization constant  $A_\gamma = 0.37$  and the spectral index  $\alpha = 2.3$  (blue curves). Our model fits the flare data very well up to energy  $E_\gamma \sim 1\text{ TeV}$  and above this energy the flux falls faster than the observed data. Above  $\sim 500\text{ GeV}$ ,  $F_{\gamma,\text{int}}$  (upper blue curve) falls faster than the MAGIC fit, which is a constant. This fall in the  $F_{\gamma,\text{int}}$  is also responsible for the faster fall in the  $F_{\gamma,\text{obs}}$  in the energy range  $\sim 500\text{ GeV}$  to  $1.2\text{ TeV}$  even if the fall in  $e^{-\tau_{\gamma\gamma}}$  is slow. Above  $E_\gamma \sim 1.2\text{ TeV}$ , the linear growth in  $\tau_{\gamma\gamma}$  wins over the fall in the  $F_{\gamma,\text{int}}$  so that the fall in the  $F_{\gamma,\text{obs}}$  is slowed down. For comparison we have also shown the log-parabola fit by the MAGIC collaboration (lower magenta dashed curve); however, both these fits are poor above  $\sim 700\text{ GeV}$ .

We have also plotted  $F_{\gamma,\text{obs}}$  and  $F_{\gamma,\text{int}}$  for SED-II in Lep-A. Here a good fit is obtained for  $A_\gamma = 0.64$  and  $\alpha = 2.6$  (lower black curve). We observed that the MAGIC fit to  $F_{\gamma,\text{int}}$  and our result (upper black curve) are the same and constant in the whole energy range. In the photohadronic model, above  $\sim 1\text{ TeV}$  the  $F_{\gamma,\text{obs}}$  has a slow fall even though the  $F_{\gamma,\text{int}}$  is constant for all energies. Again the curve changes

its behavior above  $\sim 1.2$  TeV. This peculiar behavior is due to the slow growth of  $\tau_{\gamma\gamma}$  in the range  $600 \text{ GeV} \leq E_\gamma \sim 1.2$  TeV and above this energy shows an almost linear growth. The comparison of the  $F_{\gamma,\text{obs}}$  in SED-I and SED-II shows a marked difference for  $E_\gamma > 0.8$  TeV. The lower black curve (SED-II) falls slower than the lower blue curve (SED-I). The higher value of  $\Phi_{\text{SSC}}$  in SED-II compared to the one in SED-I in the energy range  $115 \text{ MeV} \leq \epsilon_\gamma \leq 2.8 \text{ MeV}$  is responsible for this discrepancy, which can be seen from Fig. 2.

Again, in the photohadronic scenario and using SED-II of Lep-D, the observed flare energy range  $75.6 \text{ GeV} \leq E_\gamma \leq 3.1 \text{ TeV}$  corresponds to a background photon energy in the interval  $23.9 \text{ MeV} (5.8 \times 10^{21} \text{ Hz}) \leq \epsilon_\gamma \leq 0.58 \text{ MeV} (1.4 \times 10^{20} \text{ Hz})$  and the VHE proton energy in the range  $0.76 \text{ TeV} \leq E_p \leq 31 \text{ TeV}$ . The above range of  $\epsilon_\gamma$  lies in the tail region of the SSC spectrum, as shown in Fig. 2. In Fig. 3 we also show  $F_{\gamma,\text{obs}}$  and  $F_{\gamma,\text{int}}$  for SED-II. A good fit to the flare data is obtained by taking  $A_\gamma = 5.9$  and  $\alpha = 2.6$  (lower red curve). We observed that our model fit decreases more slowly than the MAGIC fit and the model fits of Lep-A above  $\sim 1$  TeV. The comparison of  $F_{\gamma,\text{int}}$  (upper red curve) with the MAGIC fit shows that the two are practically the same for  $E_\gamma < 2$  TeV and above this energy the photohadronic prediction increases slightly; however, there is a big difference in  $F_{\gamma,\text{obs}}$  above  $E_\gamma > 1$  TeV. From Eq. (4) we observed that both the intrinsic and the observed fluxes are proportional to  $E_\gamma^{-\alpha+3}$  and  $\Phi_{\text{SSC}}$ ; also both are independent of an exponential cut-off. However, if at all there is a cut-off energy it must be  $E_{\gamma,c} \geq 70$  TeV, otherwise the  $F_{\gamma,\text{obs}}$  will fall faster than the predicted fluxes shown in black and red lower curves in Fig. 3, which will be non-compatible with the flare data.

The 1ES 1011+496 has a central black hole of mass  $M_{\text{BH}} \simeq 10^{8.28} M_\odot$  corresponding to the Eddington luminosity  $L_{\text{Edd}} \simeq 2.4 \times 10^{46} \text{ erg s}^{-1}$  and a luminosity distance  $d_L$  of about 1077 Mpc. In the flaring state, in general, the flux of the individual jet can be as high as  $F_{\text{Edd}}/2$  and for the highest energy protons with  $E_p = 31$  TeV must have a flux  $F_p < F_{\text{Edd}}/2 \simeq 0.86 \times 10^{-10} \text{ erg cm}^{-2} \text{ s}^{-1}$ . This condition translates into the constraint  $\tau_{p\gamma} > 0.21$ . Also from the argument that the emission in the hidden internal jet satisfies  $L'_{\text{jet}} \gg 4\pi R_f'^2 n'_{\gamma,f} \epsilon'_\gamma$  will put an upper limit on  $\tau_{p\gamma}$ . By analyzing the above leptonic models, Lep-A (SED-I, SED-II) and Lep-D (SED-II), with different parameters we found  $R_f' < 2.8 \times 10^{14} \text{ cm}$  and  $n'_{\gamma,f} > 1.6 \times 10^{12} \text{ cm}^{-3}$  for which the proton luminosity is sub-Eddington because of the compactness of the inner jet. Due to the adiabatic expansion of the inner blob, the photon density will be reduced to  $n'_\gamma$  and also the optical depth  $\tau_{p\gamma} \ll 1$ . The energy will be dissipated once these photons cross into the bigger outer cone. This will drastically reduce the  $\Delta$ -resonance production efficiency from the  $p\gamma$  process and this is precisely the reason why in the traditional jet scenario the high energy proton flux  $F_p$  required is more than  $10^6$  times the Eddington flux

to explain the observed multi-TeV data. So the compactness of the inner jet region in the photohadronic scenario overcomes the problem of the super-Eddington energy budget faced by the traditional hadronic model.

## 6 Conclusions

The multi-TeV flaring of February–March 2014 from 1ES 1011+496 is interpreted using the photohadronic scenario. To account for the effect of the diffuse radiation background on the VHE  $\gamma$ -rays we incorporate a template EBL model to calculate the observed flux. However, the absorption of the VHE  $\gamma$ -rays within the jet is neglected by assuming that the intrinsic flux takes care of this extraneous effect. Also two different leptonic models are considered to fit the flare data and the results are compared. The spectral index  $\alpha$  is the only free parameter here. The flare data has a non-trivial shape above  $E_\gamma \sim 600$  GeV and in the photohadronic model this behavior can be explained by the slow to linear growth in  $\tau_{\gamma\gamma}$  above this energy range, complemented by a higher SSC flux. The EBL contribution alone cannot explain the non-trivial shape of the data which can be clearly seen by comparing the lower blue curve with the lower black and red curves in Fig. 3. Also a good fit to the observed data corresponds to an almost flat intrinsic flux. The compact internal jet scenario discussed here can easily overcome the problem of the energy budget faced by the standard jet scenario. A detailed analysis of the influence of SSC photons of different leptonic models and the EBL effect will be reported in a forthcoming paper. It is worth mentioning that a structured jet (spine-layer) model [41,42] with a faster and narrower spine surrounded by a slower and less collimated layer is developed to explain the high energy emission from blazars. In this framework, the layer component usually moves more slowly than the spine and the relative motion between the spine and layer will amplify the photon energy density from the spine (layer) in the frame of the layer (spine) and therefore amplify the inverse Compton emission of both the components. This model is successfully used to explain the VHE  $\gamma$ -rays emission from radio galaxies and blazars [41–43].

Towards the end of the observation period by the MAGIC telescopes, the source activity was lower, which amounted to larger uncertainties in the flux and correspondingly the average spectrum. Probably this might be the reason for larger uncertainties in the VHE range of the average spectrum. The MAGIC telescopes exposure period for most of the nights was  $\sim 40$  min, which was extended for  $\sim 2$  h on nights of 8th and 9th February [5]. This extended period of observation might have a better flux resolution and our expectation is that the photohadronic scenario will be able to fit the data well. In the future, for a better understanding of the EBL effect and the role played by the SSC photons on the VHE  $\gamma$ -ray flux

from intermediate to high redshift blazars, it is necessary to have simultaneous observations in multi-wavelength of the flaring objects.

**Acknowledgements** We thank Shigehiro Nagataki, D. Khangulyan, Yoshiyuki Inoue, Susumu Inoue, M. V. Barkov, Haoning He, Adiv Gonzalez and Lucy Fortson for many useful discussions. S.S. is a Japan Society for the Promotion of Science (JSPS) invitational fellow. The work of S.S. is partially supported by DGAPA-UNAM (Mexico) Project No. IN110815.

**Open Access** This article is distributed under the terms of the Creative Commons Attribution 4.0 International License (<http://creativecommons.org/licenses/by/4.0/>), which permits unrestricted use, distribution, and reproduction in any medium, provided you give appropriate credit to the original author(s) and the source, provide a link to the Creative Commons license, and indicate if changes were made. Funded by SCOAP<sup>3</sup>.

## References

1. J. Albert et al., [MAGIC Collaboration]. *Astrophys. J.* **667**, L21 (2007)
2. M.L. Ahnen et al., [MAGIC and AGILE Collaborations]. *Mon. Not. R. Astron. Soc.* **459**, 2286 (2016)
3. J. Aleksić et al., *Astron. Astrophys.* **591**, A10 (2016)
4. T.C. Weekes et al., *Astropart. Phys.* **17**, 221 (2002)
5. M.L. Ahnen et al., *Astron. Astrophys.* **590**, A24 (2016)
6. R. Reinthal et al., [MAGIC and AGILE Team Collaborations]. *J. Phys. Conf. Ser.* **355**, 012017 (2012)
7. A.A. Abdo et al., [Fermi LAT Collaboration]. *Astrophys. J.* **719**, 1433–1444 (2010)
8. P. Roustazadeh, M. Böttcher, *Astrophys. J.* **728**, 134 (2011)
9. G. Fossati, L. Maraschi, A. Celotti, A. Comastri, G. Ghisellini, *Mon. Not. R. Astron. Soc.* **299**, 433 (1998)
10. G. Ghisellini, A. Celotti, G. Fossati, L. Maraschi, A. Comastri, *Mon. Not. R. Astron. Soc.* **301**, 451 (1998)
11. C.D. Dermer, R. Schlickeiser, *Astrophys. J.* **416**, 458 (1993)
12. M. Sikora, M.C. Begelman, M.J. Rees, *Astrophys. J.* **421**, 153 (1994)
13. F. Aharonian et al., [HESS Collaboration]. *Astrophys. J.* **695**, L40 (2009)
14. A. Abramowski et al., [H.E.S.S. and VERITAS Collaborations]. *Astrophys. J.* **746**, 151 (2012)
15. H. Krawczynski, S.B. Hughes, D. Horan, F. Aharonian, M.F. Aller, H. Aller, P. Boltwood, J. Buckley et al., *Astrophys. J.* **601**, 151 (2004)
16. W. Cui et al., [VERITAS Collaboration]. *AIP Conf. Proc.* **745**, 455 (2005)
17. M. Blazejowski, G. Blaylock, I.H. Bond, S.M. Bradbury, J.H. Buckley, D.A. Carter-Lewis, O. Celik, P. Cogan et al., *Astrophys. J.* **630**, 130 (2005)
18. G. Cao, J. Wang, *Astrophys. J.* **783**, 108 (2014)
19. A.A. Zdziarski, M. Böttcher, *Mon. Not. R. Astron. Soc.* **450**(1), L21 (2015)
20. P. Pjanka, A.A. Zdziarski, M. Sikora, *Mon. Not. R. Astron. Soc.* **465**, 3506 (2017)
21. A. Mücke, R.J. Protheroe, *Astropart. Phys.* **15**, 121 (2001)
22. W. Essey, A. Kusenko, *Astropart. Phys.* **33**, 81 (2010)
23. W. Essey, O.E. Kalashev, A. Kusenko, J.F. Beacom, *Phys. Rev. Lett.* **104**, 141102 (2010)
24. W. Essey, O. Kalashev, A. Kusenko, J.F. Beacom, *Astrophys. J.* **731**, 51 (2011)
25. W. Essey, A. Kusenko, *Astrophys. J.* **751**, L11 (2012)
26. F. Aharonian, W. Essey, A. Kusenko, A. Prosekin, *Phys. Rev. D* **87**(6), 063002 (2013)
27. O.E. Kalashev, A. Kusenko, W. Essey, *Phys. Rev. Lett.* **111**(4), 041103 (2013)
28. W. Essey, A. Kusenko, *Astropart. Phys.* **57–58**, 30 (2014)
29. S. Sahu, A.F.O. Oliveros, J.C. Sanabria, *Phys. Rev. D* **87**, 103015 (2013)
30. S. Sahu, L.S. Miranda, S. Rajpoot, *Eur. Phys. J. C* **76**, 127 (2016)
31. S. Sahu, E. Palacios, *Eur. Phys. J. C* **75**, 52 (2015)
32. M.G. Hauser, E. Dwek, *Ann. Rev. Astron. Astrophys.* **39**, 249 (2001)
33. A. Domínguez et al., *Mon. Not. R. Astron. Soc.* **410**, 2556 (2011)
34. M.H. Salamon, F.W. Stecker, *Astrophys. J.* **493**, 547 (1998)
35. F.W. Stecker, O.C. de Jager, M.H. Salamon, *Astrophys. J.* **390**, L49 (1992)
36. A. Franceschini, G. Rodighiero, M. Vaccari, *Astron. Astrophys.* **487**, 837 (2008)
37. A. Domínguez, J.D. Finke, F. Prada, J.R. Primack, F.S. Kitaura, B. Siana, D. Paneque, *Astrophys. J.* **770**, 77 (2013)
38. A. Mücke, J.P. Rachen, R. Engel, R.J. Protheroe, T. Stanev, *Publ. Astron. Soc. Aust.* **16**, 160 (1999)
39. S. Sahu, M.V.L. Yáñez, L.S. Miranda, A.R. de León, V. Gupta, *Eur. Phys. J. C* **77**, 18 (2017)
40. F. Aharonian et al., [HEGRA Collaboration]. *Astron. Astrophys.* **406**, L9 (2003)
41. G. Ghisellini, F. Tavecchio, M. Chiaberge, *Astron. Astrophys.* **432**, 401 (2005)
42. F. Tavecchio, G. Ghisellini, *Mon. Not. R. Astron. Soc.* **385**, 98 (2008)
43. M. Sikora, M. Rutkowski, M. Begelman, *Mon. Not. R. Astron. Soc.* **457**(2), 1352 (2016)